

# 000 001 002 003 004 005 006 007 008 009 010 011 012 013 014 015 016 017 018 019 020 021 022 023 024 025 026 027 028 029 030 031 032 033 034 035 036 037 038 039 040 041 042 043 044 045 046 047 048 049 050 051 052 053 TASK REPRESENTATIONAL DYNAMICS FOR COM- POSITIONAL GENERALIZATION DURING CONTEXT- DEPENDENT COGNITIVE TASKS

006 **Anonymous authors**

007 Paper under double-blind review

## 010 ABSTRACT

013 The ability to generalize compositionally is central to intelligent behavior. While  
 014 recent work shows that networks can generalize compositionally under certain  
 015 conditions, many studies focus on simple compositional tasks, such as those that  
 016 are purely linguistic (or unimodal), or those with no temporal structure. **Here we**  
 017 **investigate how representational dynamics shape compositional generalization in**  
 018 **recurrent neural network (RNN) models during cognitive tasks with evolving tem-**  
 019 **poral structure, providing insights into neural computation during flexible reason-**  
 020 **ing.** We trained RNNs on the Concrete Permuted Rules (C-PRO) task, a cognitive  
 021 **compositional task established for humans that requires integration of information**  
 022 **across task phases.** We assessed how different learning regimes induced general-  
 023 **ization and representational dynamics.** We systematically varied model initial-  
 024 **izations to generate RNNs that exhibited a wide range of compositional gener-**  
 025 **alization performance, ranging from 38% to 90%.** Analysis of high-performing  
 026 **models revealed nontrivial temporal dynamics of task representations, highlight-**  
 027 **ing the importance of selectively engaging the right features at the appropriate task**  
 028 **phase for generalization.** Our findings reveal that successful compositional gener-  
 029 **alization requires the orchestration of structured intermediate representations that**  
 030 **are dynamically composed, resulting in complex, feature-specific representational**  
 031 **dynamics – providing testable principles for how neural systems enable flexible**  
 032 **reasoning.**

## 033 1 INTRODUCTION

035 Understanding the mechanisms underlying compositional generalization requires examining how  
 036 networks organize their internal representations during learning and task performance. Recent  
 037 work has established that neural networks can achieve compositional generalization when equipped  
 038 with useful and reusable representations (Yang et al., 2019; Ito et al., 2022; Johnston & Fusi,  
 039 2023; Driscoll et al., 2024). **Other theoretical work has identified distinct learning regimes, with**  
 040 **“rich” learning leading to structured representations that likely enhance compositional generaliza-**  
 041 **tion (Lippl & Stachenfeld, 2024), while “lazy” models learn input-output mappings by projecting**  
 042 **input features to a random, high-dimensional space, similar to reservoir computing (Chizat et al.,**  
 043 **2019).** However, these prior studies have primarily examined the structure of representations with-  
 044 **out considering cognitive tasks that require the temporal orchestration of information, and have**  
 045 **typically focused on simple categorization or context-dependent tasks with limited manipulation of**  
 046 **task features.** This limits the insights from prior studies to more practical settings, where decisions  
 047 **in realistic cognitive tasks unfold over time and require dynamic integration of evolving information.**  
 048 **Thus, a computational understanding of how representational dynamics and learning regimes jointly**  
 049 **influence compositional generalization remains limited.**

050 When computational experiments are paired with well-designed cognitive tasks, they can help un-  
 051 cover the mechanisms underlying specific cognitive processes. Here, we study computational mod-  
 052 **els performing the Concrete Permuted Rules Operation (C-PRO) task, a task commonly used to**  
 053 **probe compositionality in humans. Successful C-PRO performance requires 1) composability across**  
 054 **diverse feature domains, and 2) dynamic integration of these features within and across distinct tem-**  
 055 **poral phases.** Characterizing how models perform this task extends prior work by tracking how

054 representations of context, stimuli, and response information evolve to support compositional gen-  
 055 eralization.

056 A promising approach for understanding these dynamics is through the lens of neural representa-  
 057 tional dimensionality **and decoding** (Badre et al., 2021). Studies have shown that high-dimensional,  
 058 decodable representations during stimulus integration improve task performance (Rigotti et al.,  
 059 2013; Fusi et al., 2016; Kikumoto & Mayr, 2020), while compressed, lower-dimensional abstract  
 060 representations enable generalization (Bernardi et al., 2020; Flesch et al., 2022; Ito & Murray, 2023;  
 061 Chakravarthula et al., 2025). These findings may appear contradictory, but prior studies primar-  
 062 ily characterized representational geometry during isolated task phases (e.g., instruction period vs.  
 063 stimulus presentation). We adjudicate these differences by tracking the evolution of **dimensionality**  
 064 **and decodability** across all phases, assessing their impact on compositional generalization.

065 We trained RNNs on the C-PRO task to examine how rich vs. lazy learning regimes affect rep-  
 066 resentational dynamics and compositional generalization. Consistent with prior work, rich learning  
 067 led to significantly better generalization. However, while previous work has emphasized that rich  
 068 learning tends to produce low-dimensional, structured representations that support generalization  
 069 (Flesch et al., 2022; Ito & Murray, 2023; Farrell et al., 2023; Liu et al., 2023), our findings revealed  
 070 that examining the geometry of feature-specific representations – specifically stimulus, context, and  
 071 response information – provides critical insights into compositional generalization in tasks with dy-  
 072 namic temporal structure. Specifically, we found that successful generalization emerged through  
 073 coordinated temporal dynamics across feature representations. High-performing rich networks dis-  
 074 played feature representations that expanded and compressed throughout different task phases, while  
 075 lazy networks showed relatively simplistic temporal dynamics. Interestingly, the dynamic coordina-  
 076 tion observed in rich networks enabled the formation of contingency representations that enabled the  
 077 formation of early and efficient decisions. Together, these findings demonstrate that compositional  
 078 generalization in temporally structured tasks depends on the development of structured, feature-  
 079 specific temporal dynamics.

## 080 2 EXPERIMENTAL DESIGN

### 081 2.1 THE CONCRETE PERMUTED RULES OPERATION TASK

082 The C-PRO paradigm studies context-dependent compositionality, executive control, and task gen-  
 083 eralization in humans (Ito et al., 2017; Cole et al., 2013). C-PRO composes task rules from three  
 084 domains (logical decision, sensory semantic, and motor response) to generate up to 64 task contexts  
 085 (Fig. 1B-C). The sensory rule indicates which stimulus feature to attend (*Is it red? Is it vertical? Is*  
 086 *it high pitch? Is it periodic?*); the logic rule specifies the Boolean operation (AND/NAND/OR/NOR)  
 087 applied to two sequentially presented stimuli; and the motor rule specifies the required action (button  
 088 press with a specific finger, corresponding to four output channels in our computational implemen-  
 089 tation). **While the human C-PRO task involves naturalistic multimodal stimuli, we remapped these**  
 090 **conditions and sensory modalities to multi-hot encoded stimulus input vectors for computational**  
 091 **experiments.** Successful performance requires flexibly gating the relevant sensory dimension and  
 092 assigning motor responses according to the logical evaluation of sensory information.

093 To study the evolution and dynamics of task representations, we imposed a temporal structure mim-  
 094 icking human experiments (Fig. 1B). **The structure consists of six phases: 1) task encoding where**  
 095 **the 3-rule context is presented (1 timepoint, Rule); 2) first stimulus presentation (2 timepoints,**  
 096 **early and late, Stim1\_e and Stim1\_l); 3) first delay period for working memory and integration**  
 097 **(2 timepoints, Dly1\_e and Dly1\_l); 4) second stimulus presentation (2 timepoints, Stim2\_e and**  
 098 **Stim2\_l); 5) second delay period (2 timepoints, Dly2\_e and Dly2\_l); 6) motor response window**  
 099 **(Resp).** In our computational model, task context input remains active throughout, though we also  
 100 **examine variants where context is limited to the first timepoint (Appendix Fig. A4).**

### 101 2.2 TASK DIMENSIONS: CONTEXT, STIMULI, AND RESPONSE FEATURES

102 The C-PRO contains three task dimensions: task context, stimuli, and response features (Fig. 1C).

103 **Sensory Stimuli.** In the human experiment, stimuli were defined by four feature categories (two  
 104 visual and two auditory categories): color (red/blue), orientation (vertical/horizontal visual line),

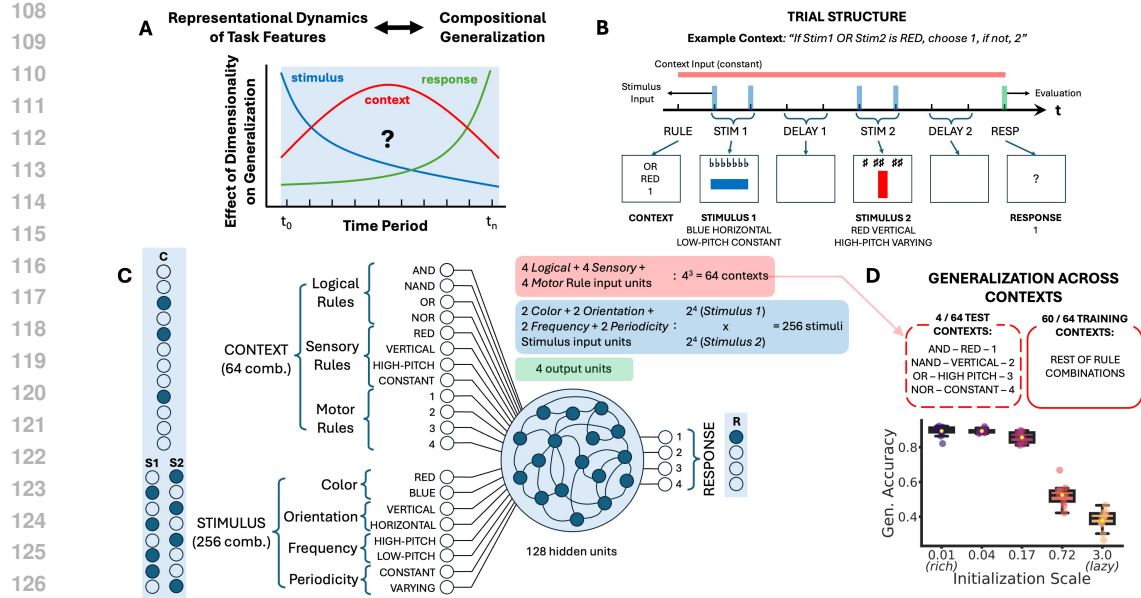


Figure 1: **Experimental overview.** We study how representational dynamics contribute to generalization in a compositional task by manipulating model initializations. **A)** We examined how dynamics of task feature representations contribute to generalization. **B)** We modeled six temporal phases within the C-PRO task: Rule encoding, Stimulus 1, Delay 1, Stimulus 2, Delay 2, and Response. Task rules compositionally combined logical operations (AND/OR/NOR/NAND), sensory features (RED/VERTICAL), and motor responses (see section 2.1). **C)** One-hot encoded inputs are projected to a 128-unit RNN initialized with either high-norm (lazy learning) or low-norm (rich learning) weights. **D)** Rich models achieved 90% generalization accuracy vs. 38% for lazy models.

frequency (high/low auditory pitch), periodicity (high/low period) (Fig. 1B). To model this computationally, we encoded each of these stimulus features as their own separate embedding dimension, represented as a multi-hot encoding. For simplicity, we defined the binary stimulus vector  $s \in \{0, 1\}^2$  for each of the four stimulus dimensions (color, orientation, frequency and periodicity). A given stimulus activated one of the two features per each category (activating four category units in total). Furthermore, the C-PRO task presented two stimuli across task phases. This resulted in  $2^4 \times 2^4 = 256$  possible stimulus combinations across the two stimuli presentations trial.

**Context.** Task context is composed from three rule domains (sensory, logical, and motor/output). Each domain has four specific rules. **Sensory rules** – RED, VERTICAL, HIGH-PITCH, CONSTANT – specify which stimulus feature to attend to or gate. These correspond to a specific color, orientation, frequency, or periodicity dimensions respectively. **Logical rules** – AND, NAND, OR, NOR – determine how to logically evaluate the gated sensory dimension across the two stimulus phases (e.g., AND  $\times$  RED  $\rightarrow$  “Are both stimuli red?”). **Motor rules** – left index, left middle, right index, right middle finger responses – specify the finger to respond with if the answer to the sensory-logical evaluation is TRUE. If the evaluation is FALSE, e.g., if the logic and sensory rules are AND and RED, but one of the stimuli is blue, then the other finger *on the same hand* is used. Computationally, a rule from each rule domain is represented as a one-hot vector  $r_x \in \{0, 1\}^4$ , for  $r_{\text{logic}}$ ,  $r_{\text{sensory}}$ ,  $r_{\text{motor}}$ . The full task context vector is specified by concatenating the vectors across each rule domain, i.e.,  $r_{\text{context}} = [r_{\text{sensory}}, r_{\text{logic}}, r_{\text{motor}}] \in \{0, 1\}^{12}$ . Permuting four rules across three rule domains results in 64 possible unique contexts (4  $\times$  4  $\times$  4 combinations):

**Motor/output vector.** Computationally, we map each finger to an embedding dimension of a one-hot vector  $o \in \{0, 1\}^4$ .

162 2.3 EVALUATING GENERALIZATION  
163

164 Our primary goal was to assess the influence of training regime and learned representational dynamics  
165 on compositional generalization. This required a subset of tasks where we 1) measured general-  
166 ization and 2) performed mechanistic analyses. Thus, model training was performed on 60/64 task  
167 contexts. Generalization and mechanistic analyses were carried out on the remaining 4 contexts.  
168 The training set was chosen such that each individual rule was equally represented across the 60  
169 training contexts. Generalization testing was then evaluated on the four remaining contexts, where  
170 each context was tested across all 256 unique trials (e.g., 256 unique stimulus combinations). Train-  
171 ing regime was manipulated through scaling the norm of the weight initialization (see Appendix A.3  
172 for further details).

173 2.4 MODEL AND DIMENSIONALITY METRIC DETAILS  
174

175 We implemented an RNN architecture with 128 hidden units, 20 input units (12 context + 8 stim-  
176 ulus), and 4 output units. The model used ReLU non-linearity with layer normalization applied  
177 before the activation function. To manipulate learning regimes, we scaled Xavier initialization  
178 weights for the recurrent connections. We tested 5 logarithmically-spaced initialization values:  
179  $\{0.01, 0.04, 0.17, 0.72, 3.0\}$ . For each initialization scale, we trained 10 networks with different ran-  
180 dom seeds, yielding 50 networks total. Training proceeded for 1000 epochs using vanilla stochastic  
181 gradient descent with a batch size of 128 and learning rate of 0.01. Each epoch comprised 15,360  
182 training examples (60 tasks  $\times$  256 stimuli per task). We include additional experiments varying  
183 model size and optimizer in the Appendix.

184 We characterized representational dimensionality at each time point separately. Representational di-  
185 mensionality measures how many dimensions are required to capture meaningful variation in neural  
186 representations. If the 64 task contexts were stored as unique contexts (i.e., each orthogonal to each  
187 other), they would span a 64-dimensional space. However, if some contexts share structure (e.g.,  
188 through overlapping rules), they can be represented in a lower-dimensional subspace. We quantified  
189 this using the participation ratio:

$$190 \quad PR = \frac{(\sum_{i=1}^s \sigma_i)^2}{\sum_{i=1}^s \sigma_i^2}$$

$$191$$

$$192$$

193 where  $\sigma_i$  represents the singular values from SVD decomposition of neural activity matrices. Higher  
194 values indicate more distributed, high-dimensional representations. We measured this metric glob-  
195 ally across all trials and separately for each feature (stimulus, context, response, contingency) by  
196 averaging activity across the other features.

197 3 RESULTS  
198

199 Networks exhibited a striking dependence on initialization scale for compositional generalization.  
200 Rich networks (smallest initialization scale) achieved 89 ( $\pm 2.9$  SD)% mean accuracy across seeds,  
201 demonstrating robust compositional generalization (see Appendix Fig. A7 for detailed breakdown).  
202 In stark contrast, lazy networks (largest initialization scale) achieved only 38 ( $\pm 5.7$  SD)% accuracy,  
203 barely above chance level (25%) (Fig. 1D), despite near-perfect training accuracy on 60 training  
204 contexts (Fig. A1). This contrast in generalization performance motivated our subsequent analyses  
205 of the internal representational dynamics underlying successful compositional generalization.

206 3.1 REPRESENTATIONAL DYNAMICS ACROSS TASK PHASES  
207

208 We quantified dimensionality of feature-specific representations (stimulus, context, response) and  
209 global dimensionality to assess representational dynamics across models (Fig. 2). Lazy networks  
210 exhibited stereotyped dynamics with dimensionality generally increasing across task phases (Fig.  
211 2D-G). In contrast, rich networks showed feature-specific heterogeneous dynamics: stimulus dimen-  
212 sionality increased during stimulus presentations then compressed after encoding both stimuli (Fig.  
213 2D); context dimensionality fluctuated with suppression during stimulus periods and re-emergence  
214 during delays (Fig. 2E); response dimensionality rose earlier in rich networks (Fig. 2F); global

216 dimensionality showed marked compression during response (Fig. 2G). These dynamics were  
 217 consistent across different model sizes (Appendix Fig. A2) and optimizers (Appendix Fig. A3).  
 218

219 To validate whether dimensionality changes reflected information content versus noise, we per-  
 220 formed cross-validated decoding of task features (Fig. 2H-K). Decoding confirmed that rich net-  
 221 works’ stimulus dimensionality expansion tracked increased decodable information (Fig. 2H). Inter-  
 222 estingly, however, high feature dimensionality did not always imply high decodability; in fact, lower  
 223 context dimensionality was associated with greater decoding accuracy, suggesting efficient compres-  
 224 sion of context information aided decodability and generalization performance (Fig. 2I). Further-  
 225 more, response information emerged independently of dimensionality changes in rich networks (Fig.  
 226 2J). Critically, context-relevant stimulus decoding revealed that rich networks selectively maintained  
 227 task-relevant dimensions while irrelevant features decayed during delays, demonstrating active fil-  
 228 tering rather than passive forgetting (Fig. 2K). Complementarily, subspace angle analysis confirmed  
 229 rich networks transiently decoupled stimulus and context subspaces during delay periods (Appendix  
 230 Fig. A6). We further quantified the cross-context representational invariance for each task feature in  
 231 rich and lazy networks across time (Appendix Fig. A5), as well as a supporting analysis using RSA  
 232 rather than decoding (Appendix Fig. A8). These distinct representational dynamics between rich  
 233 and lazy networks motivated our subsequent analysis on how these representational patterns directly  
 234 support compositional generalization.  
 235

### 3.2 REPRESENTATIONAL DYNAMICS FOR C-PRO GENERALIZATION

236 To examine how temporal variations in representational dynamics influenced generalization, we an-  
 237 alyzed how task features across different phases contributed to generalization. This was done by  
 238 performing regression analyses to predict how representational dimensionality (independent vari-  
 239 able) at each task phase contributed to generalization performance (dependent variable), with each  
 240 of the 50 models (5 initialization scales  $\times$  10 seeds) serving as a sample. This enabled us to infer  
 241 whether higher or lower representational dimensionality affected generalization across task phases.  
 242 We first analyzed how global dimensionality contributed to generalization across task phases, fol-  
 243 lowed by investigating how the dimensionality of task-specific features influenced generalization  
 244 (Fig. 3).  
 245

#### 3.2.1 GLOBAL DIMENSIONALITY DYNAMICS AND GENERALIZATION

246 Global dimensionality – which captures the overall dimensionality of trial-wise neural activity pat-  
 247 terns – revealed temporally specific relationships between dimensionality and generalization (Fig.  
 248 3A). We found that during the rule encoding phase (Rule), low dimensionality supported gen-  
 249 eralization. Following rule encoding, the initial stimulus presentation period (Stim1\_e, Stim1\_l,  
 250 Dly1\_e) exhibited the opposite pattern, where high dimensionality supported generalization. Late  
 251 task periods (Dly1\_l  $\rightarrow$  Resp) showed that increasingly lower dimensionality improved generaliza-  
 252 tion. These patterns reconcile contrasting neuroscience findings showing high-dimensional rep-  
 253 resentations support stimulus integration (Rigotti et al., 2013; Kikumoto et al., 2024) while low-  
 254 dimensional representations aid task encoding (Bernardi et al., 2020), revealing task-phase depen-  
 255 dent dimensionality requirements. Global dimensionality’s explanatory power ( $R^2$ ) showed temporal  
 256 progression: low ( $R^2 < 30\%$ ) until Dly1\_e, then increasing to  $> 90\%$  by trial end (Fig. 3B), indicat-  
 257 ing late-stage representations primarily account for generalization variance.  
 258

#### 3.2.2 FEATURE-SPECIFIC DIMENSIONALITY DYNAMICS AND GENERALIZATION

260 Next, we characterized how representational dynamics of specific task features contributed to gen-  
 261 eralization by quantifying feature-specific dimensionality (stimulus, context, response) across all  
 262 model initializations and using these as regressors predicting generalization performance. Decom-  
 263 posing global dimensionality into feature-specific components explained significantly more variance  
 264 ( $R^2 > 90\%$  from Stim1\_e through Resp; Fig. 3F) than global dimensionality alone.  
 265

266 Context dimensionality showed that improved generalization was associated with consistently low-  
 267 dimensional representations (Fig. 3D), consistent with prior work on abstract rule representations  
 268 supporting cross-context generalization (Bernardi et al., 2020; Ito et al., 2022). Decoding analysis  
 269 confirmed that low context dimensionality corresponded to higher decoding accuracy (Fig. 2I).  
 270

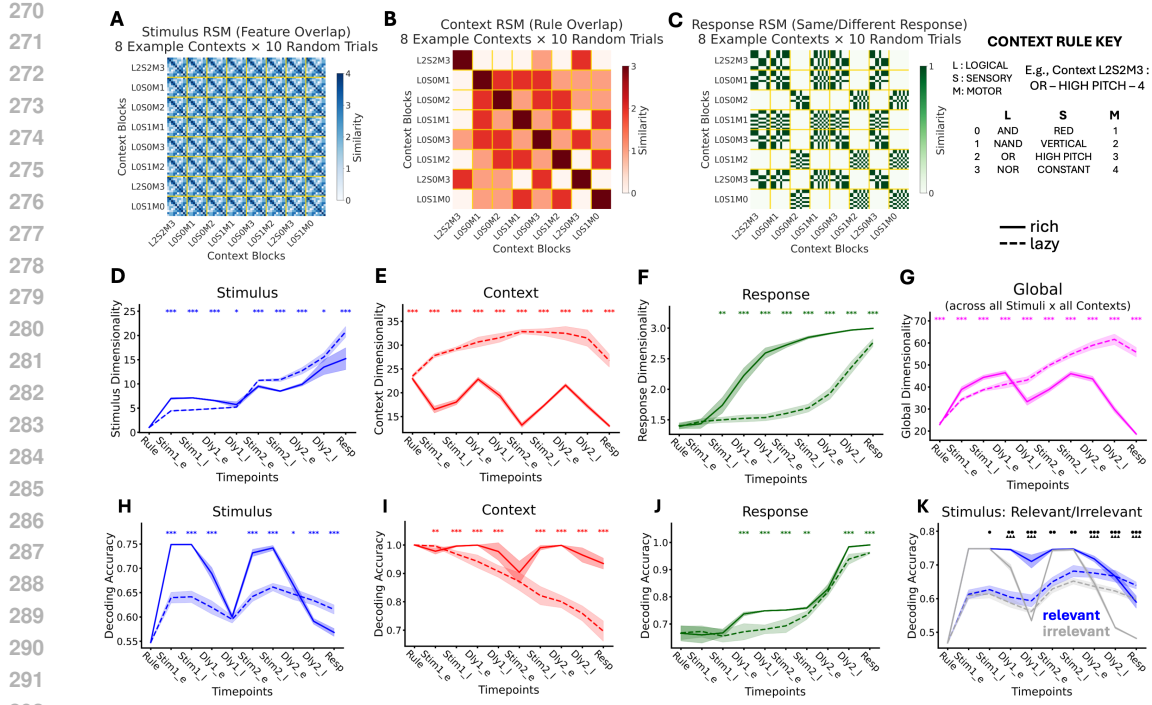


Figure 2: **Feature-specific and global representational dynamics.** We illustrate the ground truth feature similarity matrices for **A**) stimulus features, **B**) context features, and **C**) response features by computing the cosine similarity of each feature vector (either the ground truth input or output vector) across sample trials. **D-F**) Dimensionality dynamics of task-specific features in rich versus lazy networks for **D**) stimulus, **E**) context, and **F**) response. **G**) Global dimensionality measured across all 64 contexts  $\times$  256 stimulus combinations. **H-J**) Decoding traces using 10-fold cross-validation with distance-based classifiers. **H**) Rich models showed positive coupling between stimulus dimensionality and decodability. **I**) Context decodability and dimensionality show opposite relationships between regimes – rich models achieve higher decodability with lower dimensionality, while lazy models do not. **J**) Response dimensionality rises earlier in rich models, but decodable information emerges independently of dimensionality changes. **K**) Context-relevant versus -irrelevant stimulus decoding. Rich models preferentially gate and maintain relevant stimulus information (active selection); lazy models show minimal differentiation. Asterisks show FDR-corrected rich-versus-lazy comparisons (paired t-tests): \*  $p < 0.05$ , \*\*  $p < 0.01$ , \*\*\*  $p < 0.001$ . Panel K uses triangles (rich) and circles (lazy) for relevant versus irrelevant stimulus comparisons.

Stimulus dimensionality revealed dynamic temporal strategies. High dimensionality during *Stim1\_e* strongly predicted generalization (Fig. 3C), with decoding confirming dimensionality expansion tracked information content (Fig. 2H).

Response dimensionality showed high-dimensional encoding benefited generalization during rule encoding (Fig. 3E). Decoding showed response information emerged independently of dimensionality changes (Fig. 2J), with rich networks showing an earlier rise in dimensionality than lazy networks.

### 3.3 THE EFFECT OF TASK CLOSURE AND INTEGRATION ON REPRESENTATIONAL DYNAMICS

The C-PRO task structure integrates task context information with two sequentially presented stimuli. However, when studying the contributions of stimulus-related dimensionality on generalization, we observed that the first stimulus had an out-sized effect on generalization, compared to the second stimulus (Fig. 3C). This effect is likely due to the structure of the C-PRO task, where certain context and stimulus combinations enable early decision-making after the first stimulus. For example, if the task context was AND – RED – LEFT MIDDLE, corresponding to the instruction “*If Stim1*

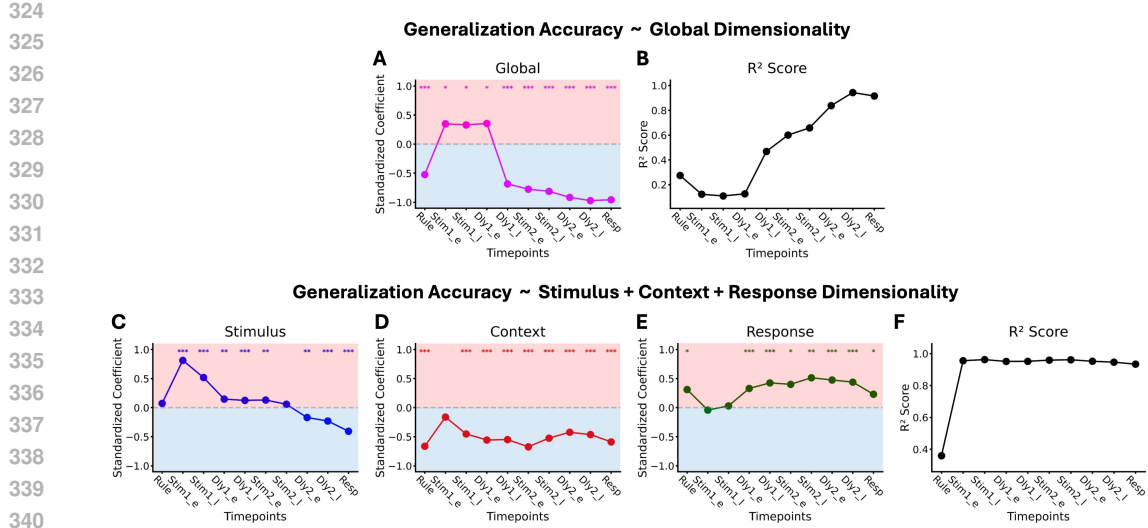
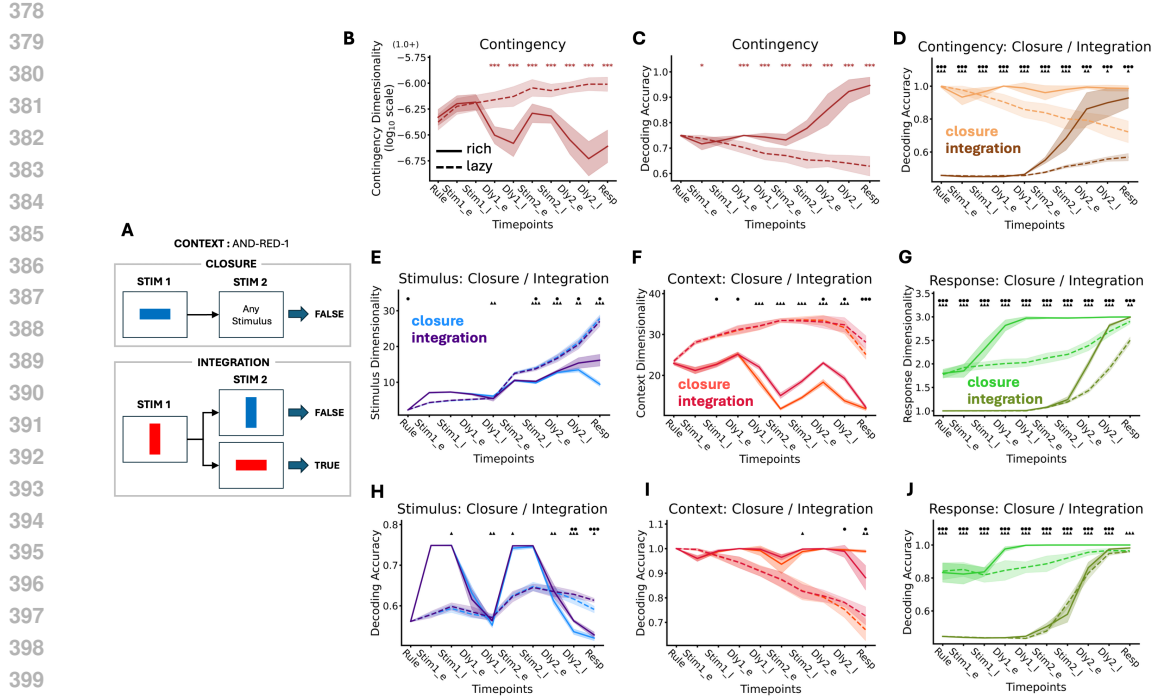


Figure 3: **Representational dynamics supporting compositional generalization.** Regression coefficients of representational dimensionality (global, stimulus, context, response) predict generalization performance across initializations. **A)** Global dimensionality coefficients: negative during rule encoding (low-dimensional improves generalization), positive during stimulus processing (high-dimensional improves), strongly negative near response (low-dimensional predicts best performance). **B)**  $R^2$  for global dimensionality: low explanatory power during early phases rises to >90% by D<sub>ly2</sub>, showing late-stage low-dimensional representations primarily account for generalization variation. **C-E)** Multiple regression isolating feature-specific dimensionality contributions. **C)** Stimulus: high-dimensional at Stim<sub>1,e</sub> transitioning to low-dimensional by D<sub>ly2</sub> predicts better generalization. **D)** Context: consistently low-dimensional predicts better generalization. **E)** Response: sustained high-dimensional after Stim<sub>1</sub> predicts better generalization. **F)** Feature-specific  $R^2$  exceeds 90% from Stim<sub>1,e</sub> through Resp, demonstrating that isolating task features better captures how representational dynamics support compositional generalization than global dimensionality alone. Asterisks show FDR-corrected comparisons of coefficients (t-test against zero): \*  $p < 0.05$ , \*\*  $p < 0.01$ , \*\*\*  $p < 0.001$ .

and Stim2 is red, press your left middle finger”, and the first stimulus was blue, then the response could be prepared after the first stimulus (Fig. 4A). This task effect has previously been described as “closure”, and leverages contingency representations – representations that enable efficient mappings to future responses/decisions (Ehrlich & Murray, 2022). We refer to trials that do not exhibit closure – tasks that require both stimuli to form the correct response – as “integration” (Fig. 4A). In this section, we characterize the representational dynamics of high-performing models during closure and integration trials. Clear dissociation of representational dynamics across these two conditions provides strong evidence that these high-performing models leverage these highly efficient contingency representations that are common for human working memory and planning (Ehrlich & Murray, 2022).

### 3.3.1 CONTINGENCY REPRESENTATION DYNAMICS

Contingency representations correspond to Boolean evaluations of sensory and logic rules (e.g., *Are both stimuli red?*), providing intermediate representations that map efficiently to motor responses (*If True, respond with X*). Rich networks showed decreased contingency dimensionality during delay periods (Fig. 4B), corresponding to high decoding accuracy during these same periods (Fig. 4C), indicating accurate encoding of the task contingency. In contrast, lazy networks showed no such contingency representations (Stim<sub>1,1</sub> → D<sub>ly1,e</sub>, Stim<sub>2,1</sub> → D<sub>ly2,e</sub>: AnovaRM interactions  $p < 0.0001$ ). Strikingly, when evaluating closure and integration trials separately, we found that rich models achieved perfect decoding accuracy after Stim<sub>1</sub> in closure trials, while integration trials reached equivalent accuracy only after Stim<sub>2</sub> (Fig. 4D). This suggests that rich networks accurately



**Figure 4: High-performing models exhibit contingency representations that enable efficient early decision-making.** **A)** CPRO task structure enables early decisions after Stim1 in "closure" trials (logical rule resolvable immediately), but not "integration" trials (requiring both stimuli). In particular, these "early decisions" can be captured through contingency representations that encode intermediate information about the task (e.g., "Are both stimuli red?" → TRUE/FALSE). **B)** Dimensionality of contingency representations. **C)** Decoding analyses of contingency representations illustrated that contingency representations tended to emerge later in the trials. **D)** However, when analyzing closure and integration trials separately, decoding contingency representations revealed that rich models achieved perfect decodability as soon as decisions can be theoretically formed (after Stim1 in closure trials; after Stim2 in integration trials). Feature-specific dimensionality for closure versus integration trials for **E)** stimulus features, **F)** context features, and **G)** response features. Decoding traces for closure versus integration trials for **H)** stimulus features, **I)** context features, and **J)** response features. Asterisks show FDR-corrected rich-versus-lazy comparisons (paired t-tests): \*  $p < 0.05$ , \*\*  $p < 0.01$ , \*\*\*  $p < 0.001$ . Panels D-J use triangles (rich) and circles (lazy) for closure versus integration comparisons.

encode intermediate contingency representations that would allow the early formation of response information. We next examine how contingency representations influence dynamics during closure versus integration trials across all task features.

### 3.3.2 REPRESENTATIONAL DYNAMICS OF CLOSURE AND INTEGRATION TRIALS

Contingency representations influenced feature-specific dynamics differently during closure (decision after Stim1) versus integration (requiring both stimuli) trials (Fig. 4E-J). Stimulus dimensionality and decoding both showed lower values during the presentation of the second stimulus when comparing closure versus integration trials (Fig. 4E,H), reflecting reduced stimulus processing when contingencies are already formed. Context dimensionality decreased in closure trials from  $Div1_e$  onwards while decoding remained at ceiling (Fig. 4F,I). Response dynamics revealed the starker contrast, and their trajectory best tracks with the emergence of decodable contingency representations: both dimensionality and decoding of response information rose immediately after Stim1 in closure trials, but only after Stim2 in integration trials (Fig. 4G,J). Together, these results provide

432 clear evidence that early response information in closure trials is enabled by the early formation of  
 433 intermediate contingency representations.  
 434

## 435 4 DISCUSSION AND CONCLUSION

438 Our findings revealed that successful compositional generalization emerges from structured repre-  
 439 sentational dynamics that enable systematic interactions between context, stimuli, and response task  
 440 features. In particular, we found that high-performing rich networks develop three key signatures:  
 441 strategic dimensionality modulation (low-dimensional context encoding, high-dimensional stimulus  
 442 processing with selective compression, and flexible response timing; Fig. 2), temporal decoupling  
 443 between stimulus and context subspaces during delay periods (Fig. A6), and efficient formation of  
 444 intermediate contingency representations that enable early decision strategies (Fig. 4, A5). These  
 445 dynamics distinguish improved generalization in rich networks from lazy networks, which exhibited  
 446 non-specific temporal dynamics across features, and failed to form reliable contingency representa-  
 447 tions critical for the correct response.

### 448 4.1 RELATED WORK

450 **Representational dynamics in models for computational neuroscience.** Prior work has demon-  
 451 strated that gradient descent optimization drives RNNs toward dimensionality compression in simple  
 452 tasks, with greater compression supporting better generalization (Farrell et al., 2022). Other work  
 453 has shown that networks trained on multiple tasks develop recurring computational motifs that en-  
 454 able compositional computation (Driscoll et al., 2024; Yang et al., 2019; Kay et al., 2024; Johnston  
 455 & Fusi, 2023; Ito et al., 2022). Our findings complement these results by revealing how feature-  
 456 specific representational dynamics – rather than global compression alone – enable compositional  
 457 generalization through stereotyped temporal dynamics of stimulus, context, and response represen-  
 458 tations.

459 **Rich and lazy learning regimes.** Our work extends the feature learning vs. function fitting trade-  
 460 off in the rich/lazy spectrum (Chizat et al., 2019; Flesch et al., 2022; Tong & Pehlevan, 2025; Lippl  
 461 & Stachenfeld, 2024; Liu et al., 2023). While prior work focused primarily on static tasks (e.g., see  
 462 Farrell et al. (2023) for review) or learning dynamics *during optimization* (Chou et al., 2025; Dominé  
 463 et al., 2024; Kunin et al., 2024; Liu et al., 2023), we examine how task feature representations  
 464 evolve *after* the model has been optimized. Critically, these systematic representational dynamics  
 465 predict generalization performance and reveal efficient, intermediary contingency representations  
 466 that enable early decision making (Ehrlich & Murray, 2022).

467 **Relation to empirical neuroscience and cognitive science.** Our findings help reconcile contrasting  
 468 views on how representational dimensionality supports task performance in empirical neuroscience.  
 469 Some studies emphasize high-dimensional representations during stimulus and delay periods for  
 470 integrating stimuli with task context (Kikumoto & Mayr, 2020; Kikumoto et al., 2024; Fusi et al.,  
 471 2016; Rigotti et al., 2013), while others highlight low-dimensional context representations as crucial  
 472 for generalization through “abstract or disentangled representations” (Bernardi et al., 2020; Flesch  
 473 et al., 2022; Courellis et al., 2024). Our results revealed that these seemingly contrasting proper-  
 474 ties reflect distinct computational phases: networks compress context representations during rule  
 475 encoding, then expand stimulus representations during integration. Crucially, we demonstrate that  
 476 feature-specific temporal coordination – not global dimensionality patterns – predicts generalization  
 477 success.

478 **Compositional generalization in the machine learning literature.** Substantial effort in machine  
 479 learning has developed benchmarks for compositional generalization (Keysers et al., 2020; Lake &  
 480 Baroni, 2018; Hupkes et al., 2020; Johnson et al., 2017; Ruis et al., 2020; Kim & Linzen, 2020;  
 481 Delétag et al., 2022), characterizing fundamental limitations of neural networks (Dziri et al., 2023;  
 482 Kim et al., 2022; Lake & Baroni, 2018) and approaches for improving generalization in lazy regimes  
 483 (Canatar et al., 2021; Abbe et al., 2024). While specialized architectures or training regimes can im-  
 484 prove compositional performance (Lake & Baroni, 2023; Csordás et al., 2022; Sinha et al., 2024;  
 485 Zhou et al., 2023; Ontanon et al., 2021; Kazemnejad et al., 2023), these benchmarks typically study  
 486 unimodal (e.g., linguistic) or static settings without the temporal integration demands of real-world  
 487 cognitive tasks. Our work differs from traditional compositionality studies in ML by focusing our

486 efforts on temporally-structured compositional paradigms established in the human literature to ad-  
 487 dress compositionality in cognitive science. While our experiments focus on a single task and ar-  
 488 chitecture (RNNs), future work should assess generalizability across diverse cognitive demands,  
 489 network architectures, and human data.

490

491

492

## 4.2 LIMITATIONS

493

494 Our study highlights the critical role of structured temporal representations in enabling robust com-  
 495 positional generalization in RNNs. Nonetheless, several limitations remain in the present work.  
 496 First, while our implementation of the C-PRO task preserves its core cognitive operations – com-  
 497 positional reasoning, working memory integration, and contingency formation – we used symbolic  
 498 input encodings (e.g., multi-hot encodings of binary features) rather than naturalistic stimuli used  
 499 in the original human task design. While this limits direct comparisons to the naturalistic sensory  
 500 processes involved in human cognition, this allowed us to isolate the cognitive processes of interest  
 501 (compositional reasoning). Nevertheless, it will be interesting for future work to explore the tem-  
 502 poral evolution of representations in compositional tasks that use naturalistic stimuli. Second, we  
 503 studied the contribution of representational dynamics to compositional generalization by manipu-  
 504 lating RNN weight initialization. While prior work has demonstrated that weight initialization can  
 505 strongly influence generalization (Chizat et al., 2019; Farrell et al., 2023), it is possible that there  
 506 are other model manipulations – as well as model architectures and optimization protocols – that in-  
 507 duce different relationships between representational dynamics and generalization that future work  
 508 can explore. Finally, we limited our investigation to the C-PRO task. While the C-PRO task has  
 509 a highly stereotyped task configuration that is commonly-used within neuroscience and cognitive  
 510 science (i.e., context → stimulus → response), it will be important to explore compositional task  
 511 designs in future work.

512

513

## 4.3 CONCLUSION

514

515 Successful compositional generalization in temporal cognitive tasks requires learning representa-  
 516 tional dynamics that enable systematic coordination across task features. Networks with different  
 517 initialization scales achieve equivalent training accuracy (>99% on trained contexts) yet show dra-  
 518 matically different generalization (90% vs. 38% on held-out contexts), allowing us to isolate which  
 519 temporal dynamics distinguish compositional success from failure. Through convergent evidence  
 520 from dimensionality, decoding, and representation analyses, we demonstrated that rich networks  
 521 coordinate temporal transformations across stimulus, context, and response features: context di-  
 522 mensionality modulates strategically across task phases including increases during working memory  
 523 delays, stimulus representations expand during presentation periods then selectively compress, and  
 524 response representations emerge with timing that reflects when decisions can be formed. Critically,  
 525 feature-specific dimensionalities predict > 90% of generalization variance from early task phases,  
 526 while global dimensionality achieves comparable predictive power only at trial end. This demon-  
 527 strates that the relevant compositional structure manifests in coordinated feature dynamics. These  
 528 dynamics also enable computational efficiency, as rich networks exploit task structure that enable  
 529 early decisions to form when possible. Together, our findings establish that successful compo-  
 530 sitional generalization emerges from temporally coordinated transformations across feature spaces  
 531 that enable systematic interactions between task features throughout processing phases.

532

## 5 REPRODUCIBILITY STATEMENT

533

534 All code and environment needed to reproduce our models, results, and figures are included in the  
 535 supplementary materials.

536

537

## REFERENCES

538

539 Emmanuel Abbe, Samy Bengio, Aryo Lotfi, and Kevin Rizk. Generalization on the unseen, logic  
 reasoning and degree curriculum. *Journal of Machine Learning Research*, 25(331):1–58, 2024.

540 David Badre, Apoorva Bhandari, Haley Keglovits, and Atsushi Kikumoto. The dimensionality of  
 541 neural representations for control. *Current Opinion in Behavioral Sciences*, 38:20–28, 2021.  
 542

543 Silvia Bernardi, Marcus K. Benna, Mattia Rigotti, Jérôme Munuera, Stefano Fusi, and C. Daniel  
 544 Salzman. The Geometry of Abstraction in the Hippocampus and Prefrontal Cortex. *Cell*, 183  
 545 (4):954–967.e21, November 2020. ISSN 0092-8674, 1097-4172. doi: 10.1016/j.cell.2020.09.  
 546 031. URL [https://www.cell.com/cell/abstract/S0092-8674\(20\)31228-9](https://www.cell.com/cell/abstract/S0092-8674(20)31228-9).  
 547 Publisher: Elsevier.

548 Abdulkadir Canatar, Blake Bordelon, and Cengiz Pehlevan. Out-of-distribution generalization in  
 549 kernel regression. *Advances in Neural Information Processing Systems*, 34:12600–12612, 2021.

550 Lakshman N. C. Chakravarthula, Takuya Ito, Alexandros Tzalavras, and Michael W. Cole.  
 551 Network geometry shapes multi-task representational transformations across human cortex,  
 552 March 2025. URL <https://www.biorxiv.org/content/10.1101/2025.03.14.643366v1>. Pages: 2025.03.14.643366 Section: New Results.

553 Lénaïc Chizat, Edouard Oyallon, and Francis Bach. On Lazy Training in Differentiable Pro-  
 554 gramming. In *Advances in Neural Information Processing Systems*, volume 32. Curran Asso-  
 555 ciates, Inc., 2019. URL <https://proceedings.neurips.cc/paper/2019/hash/ae614c557843b1df326cb29c57225459-Abstract.html>.

556 Chi-Ning Chou, Hang Le, Yichen Wang, and SueYeon Chung. Feature learning beyond the lazy-rich  
 557 dichotomy: Insights from representational geometry. *arXiv preprint arXiv:2503.18114*, 2025.

558 Michael W. Cole, Jeremy R. Reynolds, Jonathan D. Power, Grega Repovs, Alan Anticevic, and  
 559 Todd S. Braver. Multi-task connectivity reveals flexible hubs for adaptive task control. *Nature  
 560 Neuroscience*, 16(9):1348–1355, September 2013. ISSN 1546-1726. doi: 10.1038/nn.3470. URL  
 561 <https://www.nature.com/articles/nn.3470>. Publisher: Nature Publishing Group.

562 Hristos S Courellis, Juri Minxha, Araceli R Cardenas, Daniel L Kimmel, Chrystal M Reed, Taufik A  
 563 Valiante, C Daniel Salzman, Adam N Mamelak, Stefano Fusi, and Ueli Rutishauser. Abstract  
 564 representations emerge in human hippocampal neurons during inference. *Nature*, 632(8026):  
 565 841–849, 2024.

566 Róbert Csordás, Kazuki Irie, and Jürgen Schmidhuber. The Devil is in the Detail: Simple Tricks  
 567 Improve Systematic Generalization of Transformers, February 2022. URL <http://arxiv.org/abs/2108.12284> [cs].

568 Grégoire Delétang, Anian Ruoss, Jordi Grau-Moya, Tim Genewein, Li Kevin Wenliang, Elliot Catt,  
 569 Chris Cundy, Marcus Hutter, Shane Legg, Joel Veness, et al. Neural networks and the chomsky  
 570 hierarchy. *arXiv preprint arXiv:2207.02098*, 2022.

571 Clémentine CJ Dominé, Nicolas Anguita, Alexandra M Proca, Lukas Braun, Daniel Kunin, Pe-  
 572 dro AM Mediano, and Andrew M Saxe. From lazy to rich: Exact learning dynamics in deep  
 573 linear networks. *arXiv preprint arXiv:2409.14623*, 2024.

574 Laura N. Driscoll, Krishna Shenoy, and David Sussillo. Flexible multitask computation in recurrent  
 575 networks utilizes shared dynamical motifs. *Nature Neuroscience*, 27(7):1349–1363, July 2024.  
 576 ISSN 1546-1726. doi: 10.1038/s41593-024-01668-6. URL <https://www.nature.com/articles/s41593-024-01668-6>. Publisher: Nature Publishing Group.

577 Nouha Dziri, Ximing Lu, Melanie Sclar, Xiang (Lorraine) Li, Liwei Jiang, Bill Yuchen Lin, Sean  
 578 Welleck, Peter West, Chandra Bhagavatula, Ronan Le Bras, Jena Hwang, Soumya Sanyal, Xiang  
 579 Ren, Allyson Ettinger, Zaid Harchaoui, and Yejin Choi. Faith and Fate: Limits of Transformers  
 580 on Compositionality. *Advances in Neural Information Processing Systems*, 36:70293–70332,  
 581 December 2023. URL [https://proceedings.neurips.cc/paper\\_files/paper/2023/hash/deb3c28192f979302c157cb653c15e90-Abstract-Conference.html](https://proceedings.neurips.cc/paper_files/paper/2023/hash/deb3c28192f979302c157cb653c15e90-Abstract-Conference.html).

582 Daniel B. Ehrlich and John D. Murray. Geometry of neural computation unifies working memory  
 583 and planning. *Proceedings of the National Academy of Sciences*, 119(37):e2115610119, Septem-  
 584 ber 2022. doi: 10.1073/pnas.2115610119. URL <https://www.pnas.org/doi/abs/10.1073/pnas.2115610119>. Publisher: Proceedings of the National Academy of Sciences.

594 Matthew Farrell, Stefano Recanatesi, Timothy Moore, Guillaume Lajoie, and Eric Shea-Brown.  
 595 Gradient-based learning drives robust representations in recurrent neural networks by balancing  
 596 compression and expansion. *Nature Machine Intelligence*, 4(6):564–573, June 2022. ISSN 2522-  
 597 5839. doi: 10.1038/s42256-022-00498-0. URL <https://www.nature.com/articles/s42256-022-00498-0>. Publisher: Nature Publishing Group.

598

599 Matthew Farrell, Stefano Recanatesi, and Eric Shea-Brown. From lazy to rich to exclusive task  
 600 representations in neural networks and neural codes. *Current Opinion in Neurobiology*, 83:  
 601 102780, December 2023. ISSN 0959-4388. doi: 10.1016/j.conb.2023.102780. URL <https://www.sciencedirect.com/science/article/pii/S0959438823001058>.

602

603

604 Timo Flesch, Keno Juechems, Tsvetomira Dumbalska, Andrew Saxe, and Christopher Summerfield.  
 605 Orthogonal representations for robust context-dependent task performance in brains and neural  
 606 networks. *Neuron*, 110(7):1258–1270.e11, April 2022. ISSN 0896-6273. doi: 10.1016/j.neuron.  
 607 2022.01.005. URL [https://www.cell.com/neuron/abstract/S0896-6273\(22\)00005-8](https://www.cell.com/neuron/abstract/S0896-6273(22)00005-8). Publisher: Elsevier.

608

609 Stefano Fusi, Earl K Miller, and Mattia Rigotti. Why neurons mix: high dimensionality for  
 610 higher cognition. *Current Opinion in Neurobiology*, 37:66–74, April 2016. ISSN 0959-4388.  
 611 doi: 10.1016/j.conb.2016.01.010. URL <https://www.sciencedirect.com/science/article/pii/S0959438816000118>.

612

613 Peiran Gao, Eric Trautmann, Byron Yu, Gopal Santhanam, Stephen Ryu, Krishna Shenoy, and Surya  
 614 Ganguli. A theory of multineuronal dimensionality, dynamics and measurement. *BioRxiv*, pp.  
 615 214262, 2017.

616

617 Xavier Glorot and Yoshua Bengio. Understanding the difficulty of training deep feedforward neural  
 618 networks. In *Proceedings of the thirteenth international conference on artificial intelligence and  
 619 statistics*, pp. 249–256. JMLR Workshop and Conference Proceedings, 2010.

620

621 Dieuwke Hupkes, Verna Dankers, Mathijs Mul, and Elia Bruni. Compositionality Decomposed:  
 622 How do Neural Networks Generalise? *Journal of Artificial Intelligence Research*, 67:757–795,  
 623 April 2020. ISSN 1076-9757. doi: 10.1613/jair.1.11674. URL <https://www.jair.org/index.php/jair/article/view/11674>.

624

625 Takuya Ito and John D. Murray. Multitask representations in the human cortex transform along a  
 626 sensory-to-motor hierarchy. *Nature Neuroscience*, 26(2):306–315, February 2023. ISSN 1546-  
 627 1726. doi: 10.1038/s41593-022-01224-0. URL <https://www.nature.com/articles/s41593-022-01224-0>. Publisher: Nature Publishing Group.

628

629 Takuya Ito, Kaustubh R. Kulkarni, Douglas H. Schultz, Ravi D. Mill, Richard H. Chen, Levi I.  
 630 Solomyak, and Michael W. Cole. Cognitive task information is transferred between brain re-  
 631 gions via resting-state network topology. *Nature Communications*, 8(1):1027, October 2017.  
 632 ISSN 2041-1723. doi: 10.1038/s41467-017-01000-w. URL <https://www.nature.com/articles/s41467-017-01000-w>. Publisher: Nature Publishing Group.

633

634 Takuya Ito, Tim Klinger, Doug Schultz, John Murray, Michael Cole, and Mattia Rigotti. Compo-  
 635 sitional generalization through abstract representations in human and artificial neural networks.  
 636 In S. Koyejo, S. Mohamed, A. Agarwal, D. Belgrave, K. Cho, and A. Oh (eds.), *Advances in  
 637 Neural Information Processing Systems*, volume 35, pp. 32225–32239. Curran Associates, Inc.,  
 638 2022. URL [https://proceedings.neurips.cc/paper\\_files/paper/2022/file/d0241a0fb1fc9be477bdfde5e0da276a-Paper-Conference.pdf](https://proceedings.neurips.cc/paper_files/paper/2022/file/d0241a0fb1fc9be477bdfde5e0da276a-Paper-Conference.pdf).

639

640 Justin Johnson, Bharath Hariharan, Laurens Van Der Maaten, Li Fei-Fei, C Lawrence Zitnick, and  
 641 Ross Girshick. Clevr: A diagnostic dataset for compositional language and elementary visual  
 642 reasoning. In *Proceedings of the IEEE conference on computer vision and pattern recognition*,  
 643 pp. 2901–2910, 2017.

644

645 W. Jeffrey Johnston and Stefano Fusi. Abstract representations emerge naturally in neural net-  
 646 works trained to perform multiple tasks. *Nature Communications*, 14(1):1040, February 2023.  
 647 ISSN 2041-1723. doi: 10.1038/s41467-023-36583-0. URL <https://www.nature.com/articles/s41467-023-36583-0>. Publisher: Nature Publishing Group.

648 Kenneth Kay, Natalie Biderman, Ramin Khajeh, Manuel Beiran, Christopher J Cueva, Daphna  
 649 Shohamy, Greg Jensen, Xue-Xin Wei, Vincent P Ferrera, and LF Abbott. Emergent neural dynam-  
 650 ics and geometry for generalization in a transitive inference task. *PLOS Computational Biology*,  
 651 20(4):e1011954, 2024.

652 Amirhossein Kazemnejad, Inkit Padhi, Karthikeyan Natesan Ramamurthy, Payel Das, and Siva  
 653 Reddy. The impact of positional encoding on length generalization in transformers. *Advances*  
 654 *in Neural Information Processing Systems*, 36:24892–24928, 2023.

655 Daniel Keysers, Nathanael Schärli, Nathan Scales, Hylke Buisman, Daniel Furrer, Sergii Kashubin,  
 656 Nikola Momchev, Danila Sinopalnikov, Lukasz Stafiniak, Tibor Tihon, Dmitry Tsarkov, Xiao  
 657 Wang, Marc van Zee, and Olivier Bousquet. Measuring Compositional Generalization: A Com-  
 658 prehensive Method on Realistic Data, June 2020. URL <http://arxiv.org/abs/1912.09713> [cs].

659 660

661 Atsushi Kikumoto and Ulrich Mayr. Conjunctive representations that integrate stimuli, responses,  
 662 and rules are critical for action selection. *Proceedings of the National Academy of Sciences*,  
 663 117(19):10603–10608, May 2020. doi: 10.1073/pnas.1922166117. URL <https://www.pnas.org/doi/abs/10.1073/pnas.1922166117>. Publisher: Proceedings of the Na-  
 664 tional Academy of Sciences.

665 666

667 Atsushi Kikumoto, Apoorva Bhandari, Kazuhisa Shibata, and David Badre. A transient high-  
 668 dimensional geometry affords stable conjunctive subspaces for efficient action selection. *Nature*  
 669 *Communications*, 15(1):8513, 2024.

670 671

672 Najoung Kim and Tal Linzen. Cogs: A compositional generalization challenge based on semantic  
 673 interpretation. *arXiv preprint arXiv:2010.05465*, 2020.

674 675

676 Najoung Kim, Tal Linzen, and Paul Smolensky. Uncontrolled Lexical Exposure Leads to Overes-  
 677 timation of Compositional Generalization in Pretrained Models, December 2022. URL <http://arxiv.org/abs/2212.10769> [cs].

678 679

680 Nikolaus Kriegeskorte, Marieke Mur, and Peter A Bandettini. Representational similarity analysis-  
 681 connecting the branches of systems neuroscience. *Frontiers in systems neuroscience*, 2:249, 2008.

682 683

684 D Kunin, A Ráventós, C Dominé, F Chen, D Klindt, A Saxe, and S Ganguli. Get rich quick: exact  
 685 solutions reveal how unbalanced initializations promote rapid feature learning, october 2024. URL  
 686 <http://arxiv.org/abs/2406.06158>, 2024.

687 688

689 Brenden Lake and Marco Baroni. Generalization without Systematicity: On the Compositional  
 690 Skills of Sequence-to-Sequence Recurrent Networks. In *Proceedings of the 35th Interna-  
 691 tional Conference on Machine Learning*, pp. 2873–2882. PMLR, July 2018. URL <https://proceedings.mlr.press/v80/lake18a.html>. ISSN: 2640-3498.

692 693

694 Brenden M. Lake and Marco Baroni. Human-like systematic generalization through a meta-  
 695 learning neural network. *Nature*, 623(7985):115–121, November 2023. ISSN 1476-  
 696 4687. doi: 10.1038/s41586-023-06668-3. URL <https://www.nature.com/articles/s41586-023-06668-3>. Publisher: Nature Publishing Group.

697 698

699 Samuel Lippel and Kim Stachenfeld. The impact of task structure, representational geometry,  
 700 and learning mechanism on compositional generalization. March 2024. URL <https://openreview.net/forum?id=OrXvw1vN2E>.

701 702

703 Yuhan Helena Liu, Aristide Baratin, Jonathan Cornford, Stefan Mihalas, Eric Todd SheaBrown, and  
 704 Guillaume Lajoie. How connectivity structure shapes rich and lazy learning in neural circuits.  
 705 October 2023. URL <https://openreview.net/forum?id=s1SmYGc8ee>.

706 707

708 Santiago Ontanon, Joshua Ainslie, Vaclav Cvcek, and Zachary Fisher. Making transformers solve  
 709 compositional tasks. *arXiv preprint arXiv:2108.04378*, 2021.

710 711

712 Mattia Rigotti, Omri Barak, Melissa R. Warden, Xiao-Jing Wang, Nathaniel D. Daw, Earl K. Miller,  
 713 and Stefano Fusi. The importance of mixed selectivity in complex cognitive tasks. *Nature*, 497  
 714 (7451):585–590, May 2013. ISSN 1476-4687. doi: 10.1038/nature12160. URL <https://www.nature.com/articles/nature12160>. Publisher: Nature Publishing Group.

702 Laura Ruis, Jacob Andreas, Marco Baroni, Diane Bouchacourt, and Brenden M Lake. A benchmark  
 703 for systematic generalization in grounded language understanding. *Advances in neural informa-*  
 704 *tion processing systems*, 33:19861–19872, 2020.

705  
 706 Sania Sinha, Tanawan Premsri, and Parisa Kordjamshidi. A Survey on Compositional Learning of  
 707 AI Models: Theoretical and Experimental Practices, November 2024. URL <http://arxiv.org/abs/2406.08787>. arXiv:2406.08787 [cs].  
 708

709 William L Tong and Cengiz Pehlevan. Learning richness modulates equality reasoning in neural  
 710 networks. *arXiv preprint arXiv:2503.09781*, 2025.  
 711

712 Mia Whitefield and Christopher Summerfield. The effect of representational compression on flexi-  
 713 bility across learning in humans and artificial neural networks. In *Second Workshop on Repre-  
 714 sentational Alignment at ICLR 2025*, 2025.

715 Guangyu Robert Yang, Madhura R. Joglekar, H. Francis Song, William T. Newsome, and  
 716 Xiao-Jing Wang. Task representations in neural networks trained to perform many  
 717 cognitive tasks. *Nature Neuroscience*, 22(2):297–306, February 2019. ISSN 1546-  
 718 1726. doi: 10.1038/s41593-018-0310-2. URL <https://www.nature.com/articles/s41593-018-0310-2>. Publisher: Nature Publishing Group.  
 719  
 720

721 Hattie Zhou, Arwen Bradley, Eta Littwin, Noam Razin, Omid Saremi, Josh Susskind, Samy Bengio,  
 722 and Preetum Nakkiran. What Algorithms can Transformers Learn? A Study in Length Gener-  
 723 alization, October 2023. URL <http://arxiv.org/abs/2310.16028>. arXiv:2310.16028  
 724 [cs].  
 725

## 726 A APPENDIX

### 727 A.1 LARGE LANGUAGE MODEL USAGE

728 Claude Sonnet 4 was used to refine grammar, improve sentence structure, and enhance readability.  
 729 All substantive content and ideas remain original to the authors.  
 730  
 731

### 732 A.2 TASK DESIGN AND EXPERIMENTAL SETUP

#### 733 A.2.1 CPRO TASK STRUCTURE

734 We operationalized the Concrete Permuted Rules Operation (C-PRO) to study compositional  
 735 decision-making across a temporally structured task. The task rule/context was composed of three  
 736 distinct rule components: logical operations, sensory contexts, and motor responses. Each exper-  
 737 imental trial consisted of two sequentially presented stimuli (Stim1 and Stim2) followed by a re-  
 738 sponse period, interleaved with delay periods. The task structure incorporated 20-dimensional input  
 739 vectors with 4 stimulus dimensions (VDim1, VDim2, ADim1, ADim2), each taking 2 possible val-  
 740 ues. Input encoding used 8 dedicated embedding dimensions for stimulus features that were reused  
 741 between Stim1 and Stim2 presentations. In total, there were six task phases (Rule, Stim1, Dly1,  
 742 Stim2, Dly2, and Resp). However, there were 10 timepoints in total, as two timepoints were allo-  
 743 cated per stimulus and delay period, providing enhanced resolution for studying temporal dynamics.  
 744  
 745

746 The compositional structure of CPRO incorporated three types of rule components making up each  
 747 context. Logical rules included AND, NAND, OR, and NOR operations (4 options). Sensory rules  
 748 comprised RED, VERTICAL, HIGH-PITCH, and CONSTANT conditions (4 options). Motor rules  
 749 consisted of LIND, LMID, RIND, and RMID responses (4 options). This design yielded a total task  
 750 space of 64 unique tasks through all possible combinations of the three rule components (4 × 4 × 4).  
 751 All stimulus and context inputs are one-hot encoded.  
 752

#### 753 A.2.2 TRAINING AND GENERALIZATION SPLITS

754 We evaluated compositional generalization by training networks on 60/64 contexts (rule combina-  
 755 tions) while systematically withholding specific combinations for testing. The test set consisted of

4 contexts where each of the 12 rules occurred exactly once. This test set design required compositional generalization on novel task combinations, enabling assessment of systematic compositional generalization (Hupkes et al., 2020).

**Batch training structure.** Training data incorporated 256 unique stimulus combinations per task context, representing a  $16 \times 16$  grid of possible Stim1-Stim2 pairs. We organized training batches such that all samples in a batch belonged to a single task context, following prior precedent in Yang et al. (2019); Driscoll et al. (2024). Training batches were ordered in nested loops across logical, sensory, and motor contexts. This created a specific curriculum structure where logical and sensory contexts remained constant across 4 consecutive motor contexts before transitioning to the next logical-sensory pairing. With a batch size of 128, each task context required exactly 2 consecutive batches per context. Training data comprised of 15,360 examples per epoch (60 tasks  $\times$  256 stimuli).

**Optimization.** Training employed Stochastic Gradient Descent (SGD), using a learning rate of 0.01. Batch sizes were set to 128 for training. Networks were trained for 1000 epochs. We verified that training loss reached comparable levels across all 50 models by the final epoch (Fig. A1A,B). Loss computation was restricted to the response (Resp) timepoint using cross-entropy loss. Network performance was assessed every 100 training epochs using separate test batches of the 4 held-out generalization tasks (Fig. A1C,D).

### A.3 MODEL ARCHITECTURE AND INITIALIZATION

We implemented an RNN architecture with 128 hidden units following the standard recurrent update rule:

$$h_t = \text{ReLU}(\text{LayerNorm}(W_h h_{t-1} + W_x x_t + b_h)) \quad (1)$$

where  $W_x \in \mathbb{R}^{128 \times 20}$  transforms 20-dimensional inputs to 128-dimensional hidden representations, and  $W_h \in \mathbb{R}^{128 \times 128}$  performs the recurrent processing. Layer normalization was applied before the ReLU nonlinearity. The output stage consisted of a linear transformation followed by softmax:

$$y_t = \text{softmax}(W_y h_t + b_y) \quad (2)$$

where  $W_y \in \mathbb{R}^{4 \times 128}$  projects the hidden state to 4-class logits for classification.

Prior studies illustrated that different learning regimes can be induced by altering model initializations (Chizat et al., 2019). To characterize how representational dynamics affect compositional generalization, we systematically varied the initialization scales of recurrent weights while keeping input and output weights at PyTorch’s default uniform initialization. We tested 5 logarithmically-spaced initialization scale values in the interval [0.01, 3.0]:  $\{0.01, 0.04, 0.17, 0.72, 3.0\}$  (Flesch et al., 2022). These scales multiply normally distributed values (with mean 0, i.e.,  $\mathcal{N}(0, \sigma)$ ) to create weight distributions with  $\sigma \in \{0.0009, 0.0035, 0.015, 0.0636, 0.2652\}$ . We trained 10 networks with different random seeds for each scale, yielding 50 networks total. The rich learning condition corresponded to the smallest initialization scale (0.01), while the lazy learning condition used the largest scale (3.0). Recurrent weights were initialized according to Xavier initialization principles (Glorot & Bengio, 2010). Input layer weights maintained standard Gaussian initialization across all conditions to isolate the effects of recurrent weight scaling.

### A.4 REPRESENTATIONAL ANALYSIS METHODS

We used representational similarity analysis (RSA; Kriegeskorte et al. (2008)) to characterize how specific task features contributed to generalization. Neural activation vectors (128 units) were extracted from the recurrent hidden layer at each of the 10 timepoints during task execution. Neural activation vectors were sorted and averaged according to distinct task features. For example, for context representations, all activations corresponding to each unique context were averaged together; unit activations corresponding to specific stimulus conditions were averaged together; unit activations corresponding to trials for a specific response were averaged together.

#### A.4.1 FEATURE-SPECIFIC ANALYSES

Neural representations were analyzed across ten distinct timepoints corresponding to different task periods: Rule\_only (rule presentation), Stim1\_e and Stim1\_l (early and late Stim1 processing), Dly1\_e and Dly1\_l (early and late delay after Stim1), Stim2\_e and Stim2\_l (early and late Stim2

810 processing), Dly2\_e and Dly2\_l (early and late final delay), and Resp (response period). This temporal  
 811 decomposition provided two timepoints per stimulus and delay period for enhanced resolution  
 812 of temporal dynamics.

813 Feature-specific analysis involved decomposing neural activity into distinct functional components  
 814 through targeted averaging and singular value decomposition (SVD). Stimulus dimensionality was  
 815 computed by averaging activity across all 64 contexts for each of the 256 stimulus combinations,  
 816 creating  $(256 \times 128)$  matrices. Context dimensionality averaged activity across all 256 stimulus  
 817 combinations for each of the 64 contexts, yielding  $(64 \times 128)$  matrices. Response dimensionality  
 818 averaged activity across all trials for each of the 4 potential responses, producing  $(4 \times 128)$  matrices.  
 819 Contingency representational dimensionality was derived by averaging activity according to  
 820 logical rule satisfaction across all trials, creating  $(2 \times 128)$  matrices. For closure and integration  
 821 trials comparison, the activities of the two trial types are separately averaged into respective feature  
 822 conditions and two sets of feature dimensionalities (one for closure, another for integration cases)  
 823 are computed. Global dimensionality analysis used the complete  $(16,384 \times 128)$  matrix representing  
 824 all trials without feature-specific averaging. Participation ratios were computed from singular value  
 825 spectra to quantify effective dimensionality on each feature-specific matrix. We computed the par-  
 826 ticipation ratio as a measure of effective dimensionality of hidden representations through singular  
 827 value decomposition (SVD) of neural activity matrices. The participation ratio was calculated as  
 828

$$829 \text{PR} = \frac{(\sum_{i=1}^s \sigma_i)^2}{\sum_{i=1}^s \sigma_i^2}$$

830 where  $\sigma_i$  represents the singular values from SVD decomposition of neural activity matrices. This  
 831 metric quantifies the effective number of dimensions utilized by neural representations, with higher  
 832 values indicating more distributed, high-dimensional representations (see Gao et al. (2017) for fur-  
 833 ther details).

#### 834 A.4.2 STATISTICAL ANALYSES

835 Statistical comparisons employed repeated measures ANOVA to assess dimensionality changes  
 836 across task phases and rich versus lazy learning conditions. We performed 2-way repeated-measures  
 837 ANOVA (2 Initialization [Rich, Lazy]  $\times$  2 timepoints, AnovaRM) for all pairs of timepoints, report-  
 838 ing interaction terms. Post-hoc analyses were carried out using pairwise t-tests between rich versus  
 839 lazy learning conditions at all 10 timepoints. We corrected for multiple comparisons using false  
 840 discovery rate (FDR) correction.

841 To quantify dimensionality-generalization associations, we conducted linear regression analyses us-  
 842 ing generalization accuracy from all 50 networks (5 initialization scales  $\times$  10 seeds) as the dependent  
 843 variable and dimensionality values as regressors. Regressions were performed on each timepoint  
 844 separately, with FDR correction across tests. Feature-specific dimensionality analysis incorporated  
 845 10 separate regressions (3 features  $\times$  10 timepoints) with FDR correction across all tests. This  
 846 comprehensive statistical framework enabled robust assessment of the relationships between time-  
 847 dependent representational dimensionality and compositional generalization performance.

#### 848 A.5 REPRESENTATIONAL DYNAMICS IN RICH AND LAZY NETWORKS: TEMPORAL 849 EVOLUTION

850 High-performing and low-performing networks exhibited fundamentally different representational  
 851 dynamics, with lazy networks increasing global dimensionality over time compared to the dynamic  
 852 dimensionality patterns in rich networks. Kendall's tau between time and dimensionality (averaged  
 853 across 10 seeds) was  $\tau = 0.911$  ( $p = 2.98e-05$ ) for lazy networks versus  $\tau = -0.156$  ( $p = 0.6$ ) for rich  
 854 networks. This non-monotonicity in rich networks was evident as global dimensionality dropped  
 855 significantly lower closer to the response timepoint compared to lazy networks (FDR-corrected  $p <$   
 856 0.001).

857 Task feature analysis revealed that high-performing rich networks employed a dynamic encoding  
 858 strategy, exhibiting high stimulus dimensionality during first stimulus encoding (paired t-tests, FDR-  
 859 corrected  $p < 0.001$ ) followed by dimensionality compression after encoding both stimuli. Lazy  
 860 networks maintained their monotonic pattern (Kendall's  $\tau = 1.0$ ,  $p = 5.5e-07$ ) compared to the more  
 861 variable rich networks ( $\tau = 0.733$ ,  $p = 0.002$ ). Context dimensionality in rich networks showed

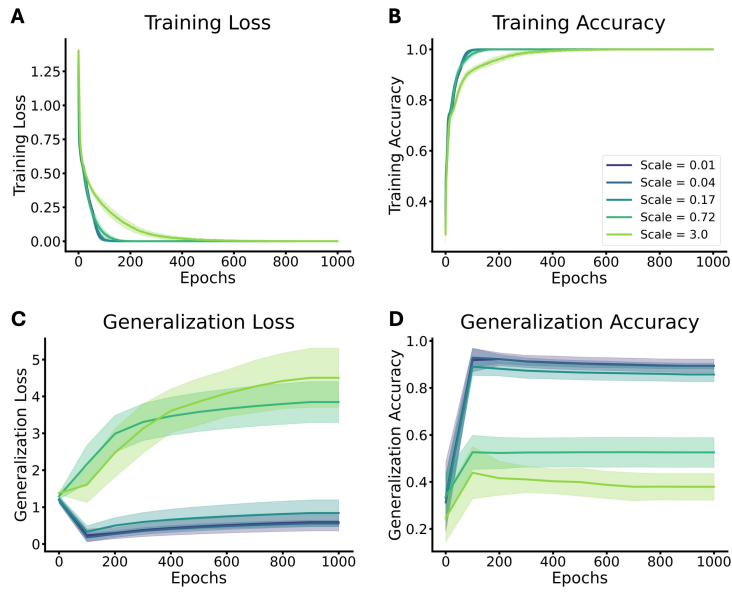
864 an inverse relationship with stimulus dimensionality—suppressed during stimulus presentation but  
 865 rising during delay periods (Spearman correlation of seed-average dimensionalities:  $\rho = -0.67$ ,  $p =$   
 866 0.033)—while lazy networks showed no such pattern ( $\rho = 0.394$ ,  $p = 0.26$ ). Despite these fluctua-  
 867 tions, rich network dimensionalities remained substantially lower than lazy networks overall (paired  
 868 t-tests, FDR-corrected  $p < 0.001$ ). The early rise in response dimensionality in rich networks sug-  
 869 gests capacity for early decision-making when feasible (paired t-tests: FDR-corrected  $p < 0.01$   
 870 starting from Stim1\_1 onwards).

871

872 **A.6 SUPPLEMENTARY FIGURES**

873

874



893

894 Figure A1: Training and generalization loss and accuracy during training. Evaluation for general-  
 895 ization was performed once every 100 epochs.

896

897

898

899

900

901

902

903

904

905

906

907

908

909

910

911

912

913

914

915

916

917

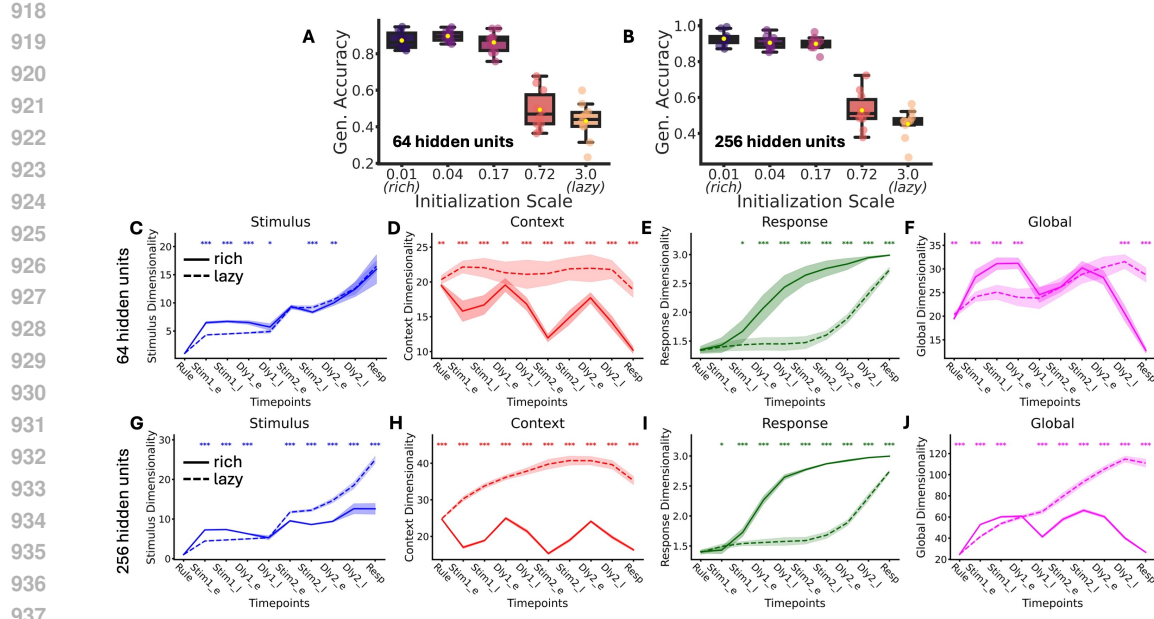


Figure A2: We reproduced the results in the main text using RNNs with 64 (A: generalization accuracy, C-F: dimensionality traces) and 256 (B: generalization accuracy, G-J: dimensionality traces) units. Both model variations reproduced patterns similar to the model with 128 units, indicating that these results are robust to model size.

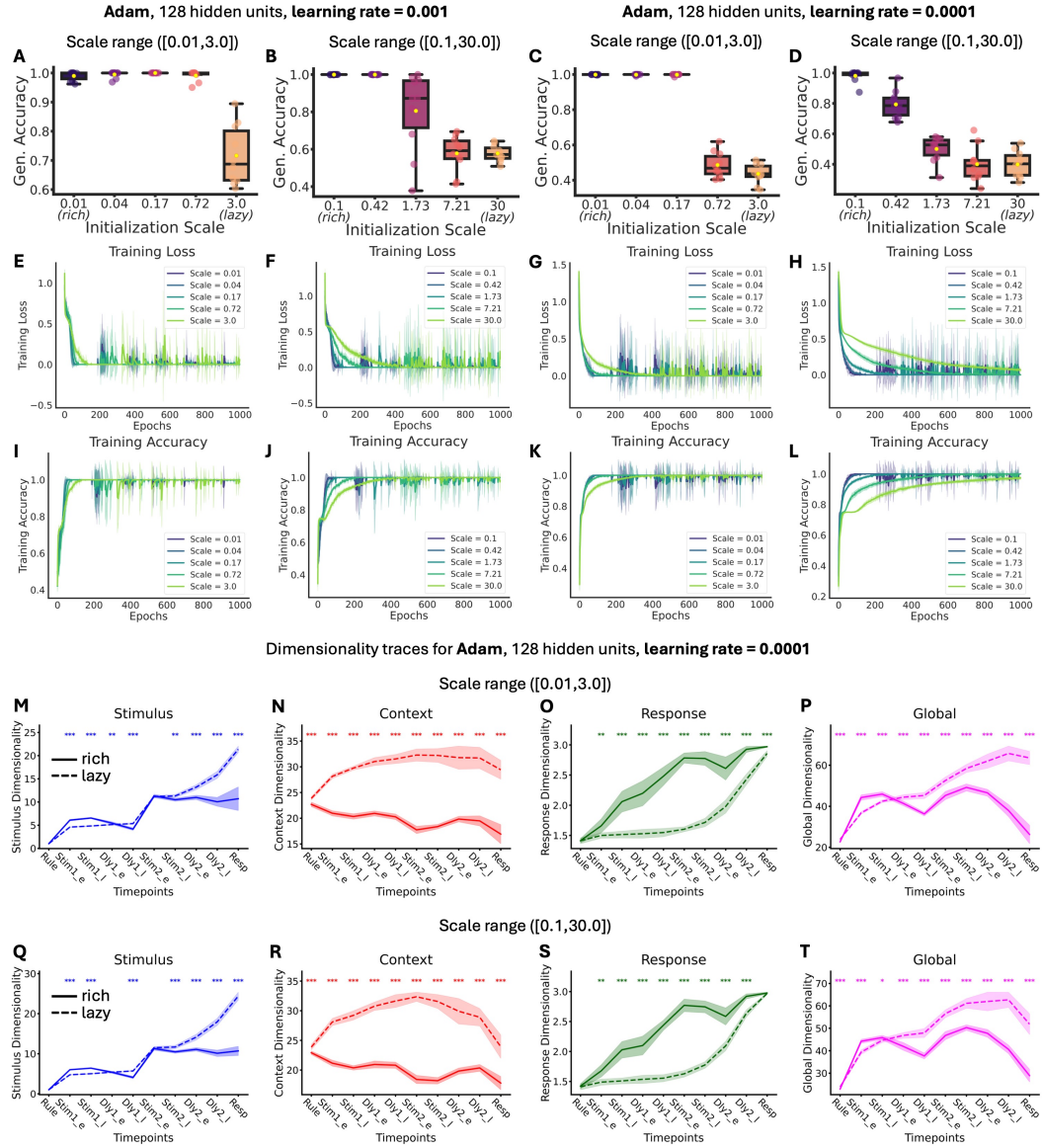
972  
973  
974  
975  
976

Figure A3: We reproduced the results in the main text using the Adam optimizer (rather than SGD in the main text). We trained networks using Adam optimizer with learning rates of 0.001 (A, E, F) and 0.0001 (C, D, G, H). **A, C:** Adam achieved near-perfect generalization ( $\geq 95\%$ ) across the original initialization scale range [0.01, 3.0], eliminating rich-lazy distinctions except at large initializations (e.g., norm of 3.0) (E, F, G, H). **B, D:** Prior work suggested that to induce lazy learning with Adam, the initialization scale needs to be magnified (Whitefield & Summerfield, 2025). Thus, as a follow-up, we expanded the initialization range to [0.1, 30.0], where we observed 'lazier' learning with larger initializations.

1023  
1024  
1025

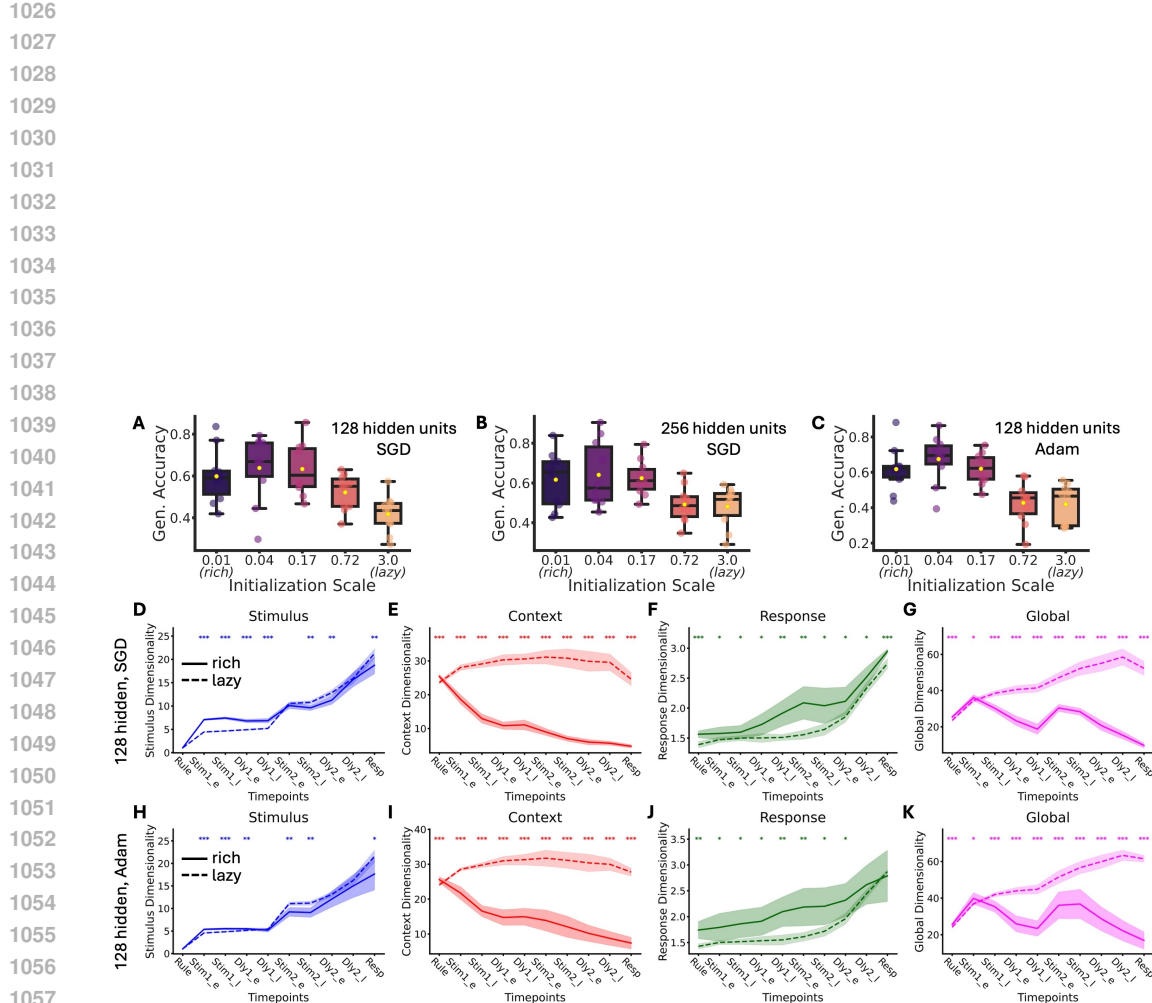


Figure A4: We evaluate model performance with a more challenging task variant, where context information is only available at  $\text{Rule}_e$  timepoint (i.e.,  $t=0$ ). This increases task difficulty as context information has to be retained over time in the model’s working memory. **A**) Richly trained models (initialization scale at 0.01 and 0.04) reached accuracy values close to 65%. (Model parameters were the same as the model used in the main text.) **B**) When the model size was increased to 256 units and number of training epochs increased to 2000, we observed similar results. **C**) Model generalization performance when using the Adam optimizer (learning rate = 0.0001, 1000 epochs). **D-G**) Dimensionality analysis plots for the model with 128 hidden units and SGD. **H-K**) Dimensionality analysis plots for the model with 128 hidden units using the Adam optimizer.

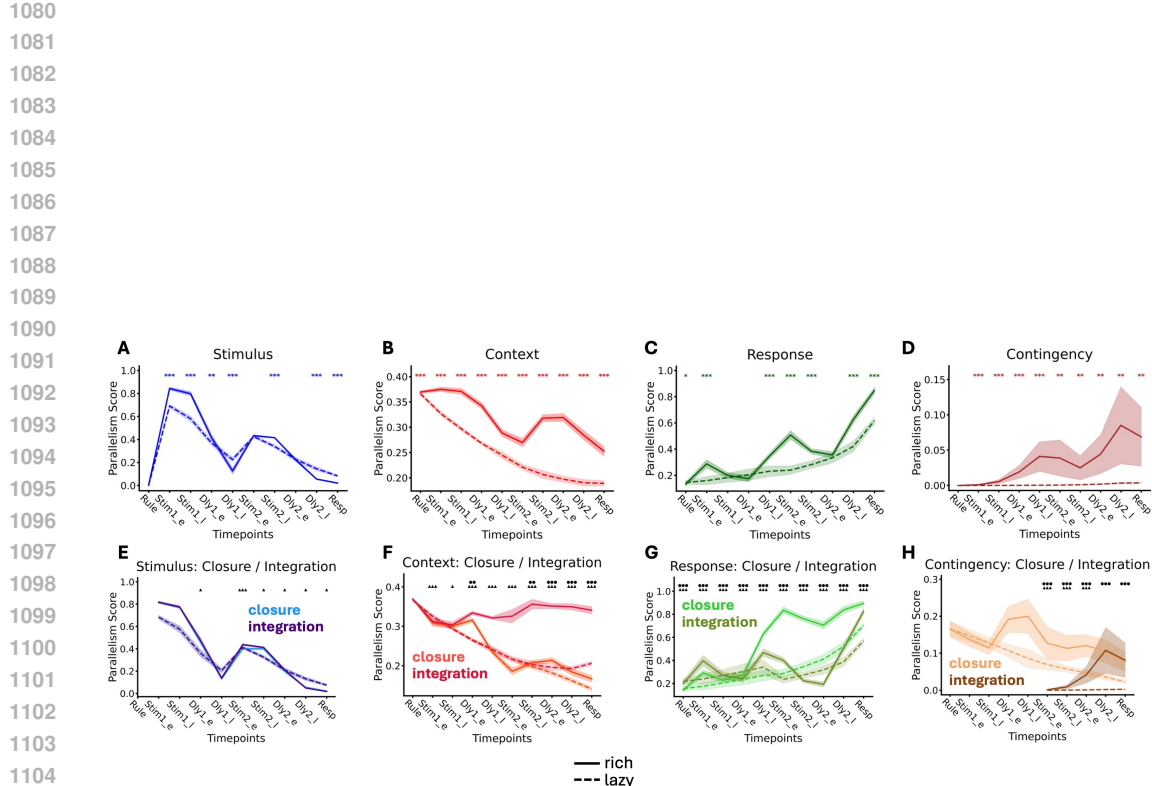


Figure A5: To measure invariance of task representations across contexts, we measured the parallelism score as a measure of representational invariance (or abstraction). Parallelism score measures the alignment of activity vectors across contexts, thereby providing information analogous to cross-condition decoding (the measure was introduced by Bernardi et al. (2020)). Parallelism scores were computed by measuring the cosine similarity between the difference of two vectors, where only a single task feature (rule, stimulus, or response) was varied, while keeping all other task conditions. Specifically, for each variable (e.g., color), we calculated difference vectors between feature values (RED vs BLUE) within the same context, then measured how parallel these vectors are across all context pairs. Higher parallelism indicates more abstract, context-invariant representations. **A,E:** Stimulus abstraction peaks during Stim1 but decreases by Stim2, indicating that stimulus representations become less invariant as integration demands increase. **B,F:** Context information maintains invariant throughout trials, but shows striking differences in closure vs. integration trials – abstraction drops when early decisions are possible, despite being decodable (cf. Figure 4I). Interestingly, this reveals that dimensionality reductions in closure trials reflect loss of invariant representations rather than information loss. **C,G:** Response abstraction increases when decisions can be formed; closure trials achieve high abstraction immediately after Stim1 while integration trials show delayed abstraction. **D,H:** Contingency abstraction mirrors response patterns — closure trials develop abstract True/False representations early and maintain them, while integration trials achieve equivalent abstraction only after Stim2 processing.

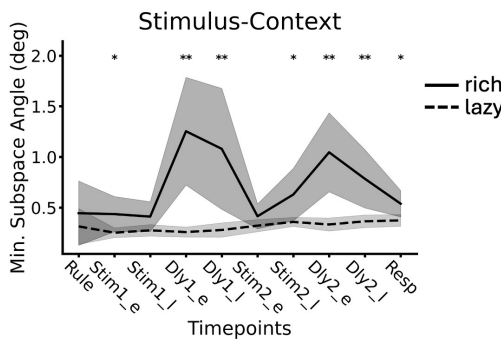


Figure A6: We measured the orthogonality between stimulus and context subspaces, and found that in rich models, stimulus and context subspaces transiently orthogonalized during delay periods. For each feature domain (stimulus and context), we computed subspace bases by using singular value decomposition (SVD) on the averaged neural activity matrices (conditions  $\times$  neurons). We retained the minimum number of principal components that explained 90% of the variance within each subspace. Principal angles between subspaces were then computed using `scipy.linalg.subspace_angles()`, with the minimum principal angle serving as our index of orthogonality. Principal angles quantify the canonical relationships between subspaces, with the minimum principal angle indicating the most aligned directions between subspaces. We chose to retain the components explaining only 90% of the variance to account for different intrinsic dimensionalities (governed by number of input latent variables) across subspaces. We observed that while the angle is overall close to zero, rich networks demonstrate slight decoupling (increase in the minimum principal angle) during delay periods, whereas lazy models do not.

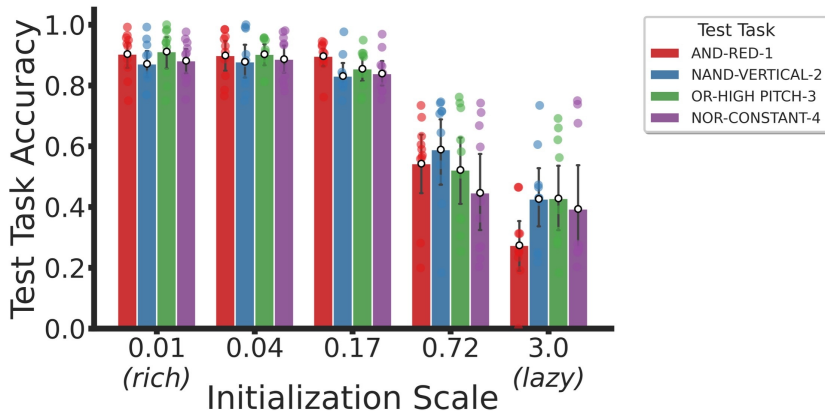


Figure A7: Generalization accuracy by each test context. We observed that rich networks demonstrated similar levels of accuracy when split across the four test contexts. Individual dots represent seeds; error bars show mean  $\pm$  SD across seeds.

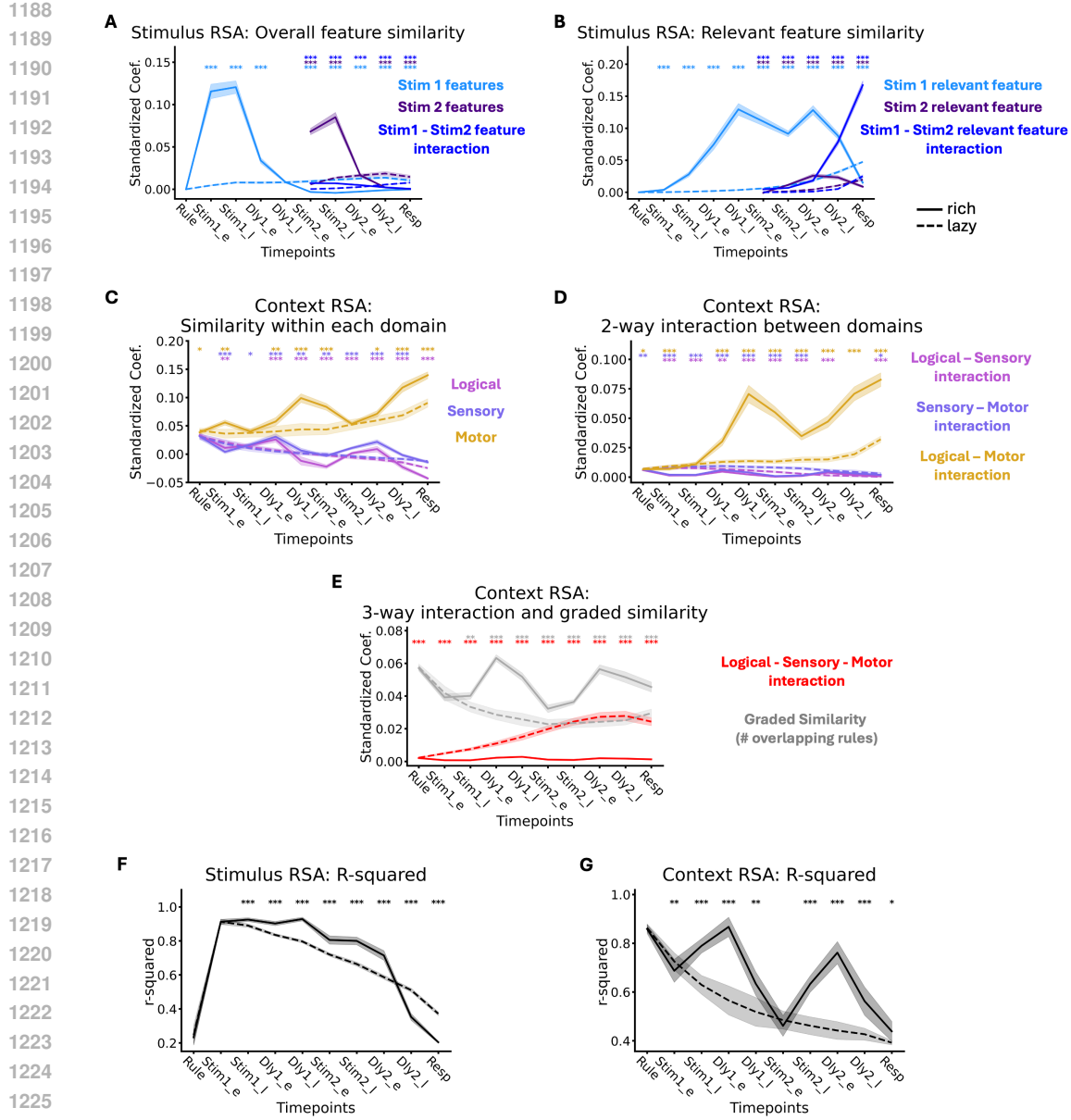


Figure A8: Stimulus and Context Representational Similarity Analysis (RSA). (A,B,F) Stimulus RSA: In each context, we computed the similarity matrix among the hidden unit representations of 256 stimulus combinations at each timepoint and tested the following six potential hypotheses together to explain the observed similarity pattern via multiple regression: **A**) Coefficients of *overall stimulus feature similarity* (similarity along the four stimulus dimensions, e.g., whether two stimulus combinations have the same color, orientation etc.) of Stimulus 1, Stimulus 2 and their interaction; **B**) Coefficients of *context-relevant stimulus feature similarity* (similarity along the color dimension if the task context involves evaluation of color dimension of the stimulus) of Stimulus 1, Stimulus 2 and their interaction. (C-E,G) Context RSA: In each context, we used the average activity across all stimulus combinations and computed similarity matrix among the 64 context representations at each timepoint and tested the following eight hypotheses to explain the observed similarity pattern via multiple regression: **C**) Coefficients of *similarity within each rule domain*, i.e., whether two contexts have the same logical or sensory or motor rule; **D**) Coefficients of *two-way similarity interactions* among the rule domains; **E**) Coefficients of *three-way similarity interaction* among the rule domains and *graded similarity*, i.e., the number of overlapping rules between two contexts irrespective of the rule domain; **F**) Coefficient of determination (r-squared) of stimulus RSA; **G**) Coefficient of determination of context RSA.